The Cryosphere Discuss., 9, 1227–1267, 2015
www.the-cryosphere-discuss.net/9/1227/2015/
doi:10.5194/tcd-9-1227-2015

The Cryosphere Discussions
Open Access

Soot on snow experiments: light-absorbing impurities effect on the natural snowpack

J. Svensson[1,2], A. Virkkula[3,1,4], O. Meinander[1], N. Kivekäs[1,5], H.-R. Hannula[6], O. Järvinen[4], J. I. Peltoniemi[4,7], M. Gritsevich[7,4,8], A. Heikkilä[1], A. Kontu[6], A.-P. Hyvärinen[1], K. Neitola[1], D. Brus[1], P. Dagsson-Waldhauserova[9,10], K. Anttila[1,7], T. Hakala[7], H. Kaartinen[7], M. Vehkamäki[11], G. de Leeuw[1,4], and H. Lihavainen[1]

[1]Finnish Meteorological Institute, Helsinki, Finland
[2]Department of Environmental Sciences, University of Helsinki, Helsinki, Finland
[3]Institute for Climate and Global Change and School of Atmospheric Sciences, Nanjing University, Nanjing, China
[4]Department of Physics, University of Helsinki, Helsinki, Finland
[5]Department of Physics, Lund University, Lund, Sweden
[6]Arctic Research Center, Finnish Meteorological Institute, Sodankylä, Finland
[7]Finnish Geospatial Research Institute, Masala, Finland
[8]Institute of Physics and Technology, Ural Federal University, Yekaterinburg, Russia
[9]Faculty of Environment, Agricultural University of Iceland, Hvanneyri, Iceland

[10]Department of Physics, University of Iceland, Reykjavik, Iceland
[11]Department of Chemistry, University of Helsinki, Helsinki, Finland

Received: 27 January 2015 – Accepted: 8 February 2015 – Published: 26 February 2015

Correspondence to: J. Svensson (jonas.svensson@fmi.fi)

Published by Copernicus Publications on behalf of the European Geosciences Union.

Discussion Paper | Discussion Paper | Discussion Paper | Discussion Paper |

Abstract

Light-absorbing impurities affect snow and ice via a decrease in albedo and a consequent disturbance to the radiative energy balance. Experimentally, these matters have only been examined in a few studies. Here we present results from a series of experiments in which we deposited different soot concentrations onto natural snow in different regions of Finland, and thereafter monitored the changes of the snowpack through the melting season. Measurements of the particulates in the snow indicated concentrations in the range of thousands of ppb to have clear effects on the snow properties, including the albedo, the physical snow characteristics, and an increased melt rate. For soot concentrations in the hundreds of ppb range, the effects were not as clearly visible, and it was more difficult to attribute the effects solely to the soot on the snow. Comparisons between our experimental data and the widely used Snow, Ice and Aerosol Radiation (SNICAR) model showed a general agreement when the model was specifically tuned to our measurements. This study highlights the importance of additional experimental studies, to further articulate and quantify the effects of light-absorbing impurities on snow.

1 Introduction

Snow has a crucial role in the Earth's radiative energy budget due to its naturally high reflectivity (or albedo) for incoming solar light. The albedo of fresh snow is 0.7–0.9 (see, e.g. review by Gardner and Sharp, 2010), which is significantly higher compared to that of other natural surfaces (Peltoniemi et al., 2010a, 2015). Snow albedo depends on many parameters, including, e.g. the snow's physical properties (such as snow grain size and snow thickness) and the wavelength range of the incoming solar radiation (Peltoniemi et al., 2010b; Wiscombe and Warren, 1980). The presence of light-absorbing impurities in snow can also have an effect on its albedo (e.g. Clarke and Noone, 1985; Warren and Wiscombe, 1980). In this paper we focus on the effect of soot on snow

properties. Soot particles, containing black carbon (BC) and organics, are strong absorbers which are produced by the incomplete combustion of fossil and bio fuels and thus originate from both anthropogenic and natural sources. With an atmospheric lifetime of roughly one week, BC has the ability to be transported over long distances far from its original emission source, e.g. the Arctic (e.g. Heintzenberg, 1982). Once it is deposited on snow, the albedo decreases and the absorption of solar radiation by the snow increases, thus leading to warming of the snow and an earlier onset of snow melt (see Fig. 29 in Bond et al. (2013) for a comprehensive schematic overview of BC's interaction with snow).

In view of the important role of BC in the climate system (revived by the influential study by Hansen and Nazarenko, 2004), ambient measurements of BC in snow have been conducted on different spatial and temporal scales in many regions of the globe. For example, in the Arctic, BC concentrations in snow have been shown to be in the range of 0–100 ppb (Doherty et al., 2010; Forsström et al., 2009, 2013; Meinander et al., 2013) and cause a perturbation to the radiative balance (Flanner et al., 2007). In the Himalayan snow and ice, with a closer proximity to major emission sources, the measured BC concentrations are higher and have been proposed to have a more pronounced negative effect on the cryosphere and the hydrological cycle (e.g. Kaspari et al., 2011; Ming et al., 2008; Xu et al., 2009).

Experimental work on BC's effect on snow is still limited to a few studies (Brandt et al., 2011; Conway et al., 1996; Hadley and Kirchstetter, 2012; Meinander et al., 2014). Conway et al. (1996) mixed high amounts (0.003–0.03 $kg\,m^{-2}$) of soot (both of hydrophilic and hydrophobic character) and volcanic ash in 10 L of snow and distributed these separate contaminant mixtures in a 2.5 cm deep layer on top of the melting snow during the melt season on Blue glacier, WA, USA. Thereafter the ablation and albedo were monitored and Conway et al. found that during the melt the soot particles were more efficiently scavenged through the snow than the volcanic ash particles. The soot particles were of submicron size while the volcanic ash particles were larger ($> 5\,\mu m$), probably explaining the difference in scavenging efficiency. Additionally, the hydropho-

bic soot particles were less efficiently scavenged through the snow than the hydrophilic soot particles. Nonetheless, the remaining fraction of soot particles at the surface still caused a clear reduction in albedo (30 % less for the contaminated snow as compared to the natural snow) and an increase in ablation rate of 50 % on the glacier surface, compared to the non-contaminant glacier surface.

The experimental approach used by Brandt et al. (2011) was based on two artificial snowpacks created with a snow gun on an open field with and without added soot. Snow samples were collected and analyzed for their BC concentration with a filter-based method (filters analyzed optically). With the combined BC concentration and the measured snow grain size, the authors calculated the albedo reduction of the snowpack in a radiative transfer model, confirming the negative effect of BC on the snowpack albedo. Hadley and Kirchstetter (2012) produced pure and BC contaminated artificial snowpacks in a laboratory experiment to study the effects of BC on snow albedo. With BC concentrations in the range of ambient measurements, BC was found to reduce snow albedo, with the BC effects amplified when the snow grain size was increased. This study also verified the widely used Snow, Ice and Aerosol Radiation (SNICAR) model (Flanner et al., 2007).

While Conway et al. (1996) focused on the mobility of soot and ash particles through the snowpack during glacier melt, using very high concentrations of impurities on the snow; Brandt et al. (2011) had 2500 ppb BC contaminated snow and its measured albedo reduction verified a radiative transfer model. Hadley and Kirchstetter (2012) had a range of different BC levels and snow grain sizes investigated to confirm the reduction of BC on snow albedo in a controlled laboratory environment.

In view of the importance of BC on snow properties and the current uncertainties, the Finnish Meteorological Institute (FMI) organized series of experiments to study the effects of Soot on Snow (SoS). This set of experiments was conducted in different regions of Finland, on natural snow with soot deposited in a controlled way. Soot was used to replicate combustion generated aerosol, which would naturally exist in the snowpack compared to aerosol composed of solely BC, which would rarely occur. The soot was

deposited on the snow by spraying it in the air as described in Sect. 2.2 and permitted to settle. This set up allowed for sampling of the airborne soot and determine its physical properties. After deposition the effect of soot on the snow albedo and the snow physical characteristics was studied throughout the entire melting season. Some of our data were compared with the SNICAR model (Flanner et al., 2007). In this paper, the experiments and results related to the broadband albedo, snow physical properties and soot measurements are presented, as well as the comparison to the SNICAR model. The focus is on the effects of the artificial impurities right after deposition, without further snow-soot interaction processes. Other relevant SoS results include the effects of impurities on the snow detailed bidirectional reflectance factor (BRF) (Peltoniemi et al., 2015), and on properties of melting snow (Meinander et al., 2014).

The approach used to deposit the soot onto the snow in our experiments can be considered to simulate artificial dry deposition onto the snowpack. The high soot concentrations used in our first experiments are unlikely to occur in ambient conditions. But on the other hand, events with dry deposition of large amounts of other light-absorbing impurities, such as dust, have been observed to naturally occur in locations prone to dust suspension (e.g. Iceland, Dagsson-Waldhauserova et al., 2014, 2015). In the latest SoS-experiment, the soot concentrations were more similar to what has been observed and measured in natural conditions (order of 100 ppb). Such results should therefore be viable for natural conditions in snow with a higher soot content (> 100 ppb) (e.g. parts of Himalaya and European Alps).

To clarify, and due to the ambiguity in the literature concerning BC terminology (see Petzold et al., 2013), we use BC in this paper in the scope of the overall discussion of light-absorbing particles and refer to elemental carbon (EC) when specifically referring to our measurement technique, used to measure the soot concentrations in the snow (thermal-optical).

2 Experiments and methods

2.1 Experiment sites

In 2011, experiments were undertaken from early March until April on a farming field (60°24′ N, 24°42′ E) near the town of Nurmijärvi, 30 km north of Helsinki, Finland. When the experiment commenced, the snowpack thickness was 50 cm and winter conditions with subzero temperatures prevailed in the area. The second experiment was conducted at the FMI observatory (60°48′ N, 23°30′ E) in Jokioinen, southern Finland, ∼ 100 km northwest of Helsinki, in February and March. At the start of the experiments, the snow depth at the site was 30 cm. The third experiment took place at the Sodankylä airfield (67°23′ N, 26°36′ E), located near the FMI Sodankylä observatory, in northern Finland, in April and May 2013. The snow depth at the experimental site was 65 cm before the soot deposition started. Hereafter the experiments in 2011, 2012 and 2013 will be referred to as SoS2011, SoS2012, and SoS2013, respectively.

2.2 Soot deposition onto the snow

Soot was deposited with different methods onto the snow surface during the experiments. In SoS2011, soot particles were produced by burning various organic materials (wood and rubber pellets from used tires) in a wood-burning stove. The smoke was lead through a pipe, cooled by snow surrounding the pipe, and lead into a rectangular chamber (3.3 m × 7.5 m × 2.8 m; width, length, height, respectively) situated on top of the snow. With this in situ production of soot, it was difficult to cool the air containing the particles before deposition and some particles were not deposited in the desired rectangular chamber. The temperature of the surface snow inside the chamber remained below freezing (visible in Fig. 1), hence, melting did not occur during the soot deposition. The deposited soot particles inside the chamber were deposited in a heterogeneous pattern (Fig. 1). An undisturbed reference site, with no impurities added, was established in close proximity (15 m) to the experimental chamber.

Because of the temperature gradient and the heterogeneous distribution pattern of the deposited soot particles in SoS2011, a different approach to deposit the soot was taken in SoS2012 and SoS2013. Soot was acquired beforehand from a chimney-sweeping company (Consti Talotekniikka) in Helsinki, which collected the soot from residential buildings with small-scale wood burning. The soot was blown into an in-house made cylindrical chamber (diameter of 4 m) carefully installed on top of the snow. The blowing system consisted of a blower, a tube blowing air into a barrel filled with the soot, and a cyclone removing particles larger than about 3 µm (the cyclone was changed between SoS2012 and SoS2013). Since the flow was not kept constant the removal of larger particles with the cyclone was only achieved with moderate success. Electron-microscopy images of particles sampled in SoS2013 after their deposition onto the snow indicate the presence of particles larger than 3 µm, most of which were some form of agglomeration consisting of carbon and some other elemental species. Several spots were made in SoS2012 and SoS2013 with varying amounts of soot. Following the deposition of soot in SoS2012, the spots were covered with 10 cm of new snow soon after the measurements began. After the snowfall (an event which included high winds as well) all of the spots had very similar albedos and the melting time of the snow depended mostly on the amount of snow in each spot. The soot analysis of the snow samples revealed that samples collected one month later contained significantly less soot (a factor of four) compared to the snow samples collected right after soot deposition. We hypothesize that the snow storm removed a large fraction of the top layer, which contained the deposited soot, and therefore no clear effects of soot on snow were observed. Any further results or analysis related to SoS2012 data will not be presented in much detail in this paper. In SoS2013 the reference spot at the airfield got contaminated during the soot deposition in the afternoon of 8 April. A new reference site, inside the airfield, was therefore created for the post depositional monitoring.

2.3 Soot characterization

The soot used in SoS2012 and SoS2013 was black with a grey character to it and therefore cannot be considered to be only containing BC particles. In SoS2012 the size distribution inside the chamber was measured with a differential mobility particle sizer (DMPS, size range 0.015–0.92 µm) and an optical particle sizer (OPS, size range 0.3–10.1 µm). It is noted that the instruments measure diameters which are defined in a different way (due to the physically different principles used for particle sizing), leading to some inconsistency in the overlapping size range. The results, however, show the occurrence of several size modes, the highest ones around 0.5–1 µm diameter. The normalized (to Ntot) size distributions did not vary much, especially in the case of OPS data. The same peaks occurred in the median values for each deposition period, as well as in the 25th and 75th percentile values.

A single particle soot photometer (SP2, Droplet Measurement Technologies, Boulder, Colorado) was also used during SoS2012. The SP2 uses a laser-incandescence method to measure the mass of individual refractory BC (rBC) from each particle (Schwarz et al., 2006; Stephens et al., 2003). It has a size range of 70–500 nm (mass-equivalent diameter assuming BC density of 1.8 g cm^{-3}), and has the capability to measure the size distribution, as well as the coating thickness of the BC particles, through the leading edge optimization method (e.g. Gao et al., 2007). The majority of the particles were coated, with an average coated to core diameter ratio of 1.5. For comparison, coated to core diameter ratios larger than 2 have been observed in aged forest fire plumes (Dahlkötter et al., 2014).

The soot characterization from SoS2012 was used for the SoS2013. The size distribution might differ slightly, as the blowing system was somewhat modified for SoS2013, with a more efficient cyclone removing the large particles. The only expected change would be that the largest particles were not measured.

2.4 Measurements of elemental carbon, albedo, and physical characteristics of the snow pack

2.4.1 Elemental carbon measurements in snow

Snow samples were collected in 5 or 7 cm increments (depending on time of sampling) and analyzed for EC and organic carbon (OC) content using a Sunset Laboratory Thermal-Optical Carbon Aerosol Analyzer (OC/EC; Birch and Cary, 1996) following the filter-based method used in e.g. Forsström et al. (2009, 2013) and Svensson et al. (2013). Briefly, the frozen snow samples were melted quickly in a microwave oven and filtered through a sterilized microquartz filter, which was then analyzed with the OC/EC using the latest recommended analysis protocol EUSAAR_2 (Cavalli et al., 2010). Uncertainties with the filter method are associated with the representativeness of the analyzed single punch (typically 1.5 cm^2) for the entire filter ($\sim$ 10 cm^2); and the efficiency of the filter to capture all of the EC particles in the liquid sample during filtering, also known as undercatch. The representativeness of the filter punch has been reported to be of the order of 20 %, based on relative SD between EC concentrations measured for different filter punches from the same filter (Svensson et al., 2013; Ruppel et al., 2014). This number is based on filters with a visible gradient of impurities on the filters. From our experience, however, the filters tend to have a uniform character (which was the case for the majority of the filters in our experiments), resulting in a much lower difference of less than 5 %, as in Ruppel et al. (2014).

Undercatch is another uncertainty issue that has been shown to take place during filtering (Doherty et al., 2010; Forsström et al., 2013; Lavanchy et al., 1999; Lim et al., 2014; Ogren et al., 1983; Torres et al., 2014). The efficiency has been shown to be very inconsistent, ranging from 10 to 95 %, between different studies and the method to evaluate the efficiency of filters. Filters have been stacked on top of each other or put in series (separated) to increase the efficiency of collecting EC (or BC with optical measurement methods) particles, both of which have recently been shown to be misleading in the actual efficiency of the filters, thus indicating a higher efficiency than

there actually is (Torres et al., 2014). Additionally, liquid samples have been measured with a different instrument (SP2) before and after filtration to observe the amount of particles percolating through the filter (Lim et al., 2014; Torres et al., 2014). It was shown that up to 90 % of the BC particles could possibly penetrate through the filter (Torres et al., 2014), while, in contrast, Lim et al. (2014) found that as little as 10 % of the BC particles could be passing through the filter. This discrepancy seems to depend on the origin of the liquid sample, and consequently the BC particles in it, as well as agglomeration processes occurring between BC particles and other light-absorbing impurities such as dust in the liquid. The majority of BC particles that are percolating through the filter during filtration seem to be smaller in size (Lim et al., 2014). In our experiments, the size distribution of the EC particles is likely to be shifted towards the larger particles (as many larger particles were observed in the electron microscopy images and also seen in the aerosol size distribution data). Therefore, we claim that we had a relatively high efficiency of our filters during filtering. Nonetheless, the EC concentrations from the experiments are probably an underestimation of the true EC concentration in the snow samples. At this time we are unfortunately not able to quantify the underestimation of EC, however, we consider it to be < 22 %, based on Forsström et al. (2013).

Snow samples for EC analysis were collected immediately following the soot deposition. In SoS2013, snow samples were additionally collected at later stages, specifically 9 and 16 days after the soot deposition. At these later sampling stages, the whole snow column was sampled in 5 cm intervals enabling us to observe any movement of the soot particles throughout the snowpack.

2.4.2 Albedo measurements

Following the deposition of soot at the designated spots, albedo measurements were set up using pyranometers measuring global irradiance (radiant flux in units $\mathrm{W\,m^{-2}}$) with a viewing angle of 2π steradians. At each spot, two pyranometers were installed horizontally: one looking upwards to measure the downwelling irradiance and another

one looking downward and hence recording the upwelling irradiance. The albedo at each measurement spot was derived as the ratio of the upwelling to the downwelling irradiance. The pyranometers employed in SoS2011 and in SoS2013 were CM11 and CMP6, respectively, manufactured by Kipp & Zonen B.V. The spectral range of the CM11 covers the wavelengths from 310 to 2800 nm, while the CMP6 covers the wavelengths 285 to 2800 nm, with the spectral response close to unity throughout the wavelength range. Following the classification given by the ISO9060:1660 and WMO (2012), CM11 and CMP6 pyranometers comply with the specifications defined for the secondary standards and high quality instruments, respectively.

In addition to this set up, BRF measurements were acquired from the sooted spots and undisturbed snow during SoS2013, using the Finnish Geodetic Institute Field Goniospectrometer (FIGIFIGO; Suomalainen et al., 2009; Peltoniemi et al., 2014). The FIGIFIGO system consists of a motor-driven moving measurement arm that tilts up to $\pm 90^{\circ}$ from the vertical, fore optics in the high end of the arm, and an ASD FieldSpec Pro FR 350–2500 nm spectroradiometer. In the beginning of each measurement sequence, the arm was first driven to the maximum (pre-defined) angle and then automatically moved to the minimum angle with constant angular speed, while making spectral measurements. The FIGIFIGO and other broadband, multiband and spectral reflectance measurements conducted during the SoS campaigns will be presented elsewhere (Peltoniemi et al., 2015; Meinander et al., 2014).

2.4.3 Snow physical characteristics measurements

In SoS2011, two snow pits were dug (one in the clean reference site and the other in the snow with the soot) on 1 April, which was approximately one month after soot deposition (Fig. 2). In the snow pits, the snow stratigraphy was physically characterized, including thickness, density, hardness (6 step hand test), grain size, and the shape. The grain sizes and types were determined using an 8x magnifying loop and a millimeter-scale grid. The reported snow grain size is the greatest extension of a grain. The snow-

type classification follows the International Classification for Seasonal Snow on the Ground (Fierz et al., 2009).

In SoS2013, the snow characteristics of the reference site were recorded during the time of the soot deposition. The snow evolution was then monitored twice during the melt season to record possible effects of BC on the snow properties with concurrent measurements of clean reference snow. The snow pits were dug in a similar manner as in SoS2011 with slight differences in the methodology of grain size determination. The snow layers were first defined based on visual and manual detection of density, hardness, and grain size differences. For each separate layer, the hardness index, wetness index, and snow grain type were defined following Fierz et al. (2009). Each snow pit had a temperature profile (every 10 cm) and a density profile (every 5 cm) recorded. For snow grain size determination, a small sample of snow for each layer was macrophotographed against a 1 mm grid. From the photographs, the average, minimum, and maximum diameter of a "typical" snow grain was then visually estimated to the closest 0.25 mm. Further, the specific surface area (SSA), defined as the surface area of the snow particles per unit mass (m^{-2} kg) (Legagneux et al., 2002), was measured with the optical instrument IceCube (A2 Photonic Sensors, France). IceCube measures the hemispherical infrared reflectance at 1310 nm of the sampled snow which can be related to snow SSA (e.g. Domine et al., 2006; Gallet et al., 2009). The measurement output is in voltages and the voltages are converted to reflectance by fitting a least squares polynomial to one background radiation and 6 reference Spectralon measurements made prior to the snow measurements. The reflectance is then converted to SSA by the use of a radiative transfer model. An error estimate on the SSA measurements is ±10–15 % based on measurement tests executed with different measurement persons and snow sampling methods.

2.5 SNICAR modeling

Our experimental data were compared with the SNICAR model (online version: http://snow.engin.umich.edu/; Flanner et al., 2007). The SNICAR model simulates the

broadband albedo of snow for different combinations of impurities (including BC, dust and volcanic ash), snow physical properties, and incident solar fluxes. SNICAR assumes snow grains and impurities have spherical shape and are sparsely distributed, ignoring thus polarization, 3-D structure of the snow pack and shapes of the grains, giving expected accuracy of ±10 %. The model was originally developed and used by Flanner et al. (2007) to estimate the global radiative effect of BC on snow, and has since then been used numerous times in other different studies of BC in snow and ice (e.g. Hadley and Kirchstetter, 2012; Kaspari et al., 2011; McConnell et al., 2007; Meinander et al., 2013; Sterle et al., 2013).

The modeled SNICAR albedo was compared to our ambient measured albedo and corresponding EC concentrations measured following the soot deposition (within a couple of hours). This comparison provides an overview of the albedo reduction caused by the soot on the snowpack immediately following soot deposition before any snow processes (including metamorphism) have started to take place. Hence, it does not provide an evaluation of the SNICAR during conditions of melt.

For input values in the SNICAR model, we used direct incident radiation and an estimated solar zenith angle (SZA; for SoS2013 61.27). The surface spectral distribution was classified as mid-latitude winter, clear-sky. The input for snow grain effective radius was derived from the measured SSA, where the SSA was converted to optical equivalent grain radius (OEGR), using the theoretical relation between OEGR and SSA (Kokhanovsky and Zege, 2004; Legagneux et al., 2002):

$$\mathrm{OEGR} = \frac{6}{\rho_{\mathrm{i}}\mathrm{SSA}} \tag{1}$$

where ρ_{i} is the density of ice. The OEGR has been suggested to closely match the grain effective radius while the conversion is sufficient for studies of hemispheric reflectance (Grenfell and Warren, 1999; Grenfell et al., 2005; Neshyba et al., 2003). For SoS2013, the conversion yielded an OEGR of 270 µm for the surface layer and 320 µm for the average of the 0–5 cm snow layer. Further, we also ran the SNICAR-model with

an effective grain radius of 750 µm, which was the visual maximum grain size (for the surface slayer), to have an upper estimate of the snow grain size measurements. The snowpack thickness was set to 65 cm, while the snow density was set to 200 kg m^{-3}. The visible and near-infrared albedos of the underlying ground were set to 0.1 and 0.3, respectively. The BC concentrations (using both the uncoated and coated BC alternative) were varied over a wide range of concentrations to imitate the wide range of EC concentrations used in our experiments. Lastly, the MAC (mass absorption cross-section) scaling factor was varied between 1.0 (corresponding to a MAC of 7.5 m^2 g^{-1} at 550 nm) and 0.3 (equivalent to a MAC of 2.25 m^2 g^{-1} at 550 nm). The lower MAC is a hypothetical number that was based on electron-microscopy images of the soot particles extracted from the snow samples, revealing the presence of many large soot particles (> 1 µm) in the snow. The size distribution from the soot characterization in SoS2012 also revealed the presence of larger sized particles which would result in a lower MAC (Bond and Bergstrom, 2005). Model runs were also made with input parameters from SoS2011, although accurate snow grain size measurements were not conducted immediately after soot deposition. Using effective grain sizes similar to those observed during SoS2013, the SoS2011 model runs did not differ much from SoS2013.

3 Results and discussion

3.1 Elemental carbon concentrations

The EC concentrations in the surface snow samples in SoS2011 varied between 120–29 000 ppb. Samples were gathered at several locations throughout the rectangular sooted snow area, and the wide range reflects the heterogeneous deposition pattern of soot inside the rectangular chamber used in the experiment. The clean reference spot had an EC surface concentration of 80 ± 31 ppb. For SoS2013, the EC concentrations from the different spots also had a wide range, 230–6400 ppb. Within each spot, at least three snow samples were collected from different parts of the spot to observe the

variation within the spot. For four of the spots, a coefficient of variation between 20 and 40 % (see Table 1) was measured. Some spots had a more homogenous deposition pattern, indicated by a variation of 8 % or lower (two spots, Table 1). The small-scale horizontal variation of EC particles within the spots is similar to what has been observed in natural conditions (Doherty et al., 2010; Forsström et al., 2013; Sterle et al., 2013; Svensson et al., 2013).

The results from the two spots that were sampled at a later stage (9 and 16 days later) are presented in Table 2. The initial average EC surface snow concentration at spot 7 was 1465 ± 26 ppb. After 9 days, the surface snow (5 cm sampling interval) contained an EC concentration of 529 ppb, accounting for 36 % of the initial EC concentration. The surface layer contained 71 % of the total EC measured for the whole snow column at that time. The majority of the remaining soot particles had at that point percolated down to 15 cm or more below the snow surface. At the last sampling (16 days after the initial soot deposition) the surface snow contained 859 ppb of EC, while the bottom snow layer contained 475 ppb. Hence, about 64 % of the total EC concentration for the snow column at this time was in the surface layer. The EC in the surface layer accounted for 59 % of the originally deposited soot. The second spot (spot 5) was also sampled at later stages and the results were similar (see Table 2). Nine days after the initial soot deposition, about 43 % of the soot was still in the surface layer, accounting for 69 % of the total EC concentration measured in the whole snow column. Similarly, after 16 days, the EC concentration in the surface snow was 45 % of the original EC concentration.

The temporal progression of EC concentrations during SoS2013 shows that the BC particles scavenging efficiency was less than 100 % with meltwater during snow melt. Ambient measurements show that BC particles and other light-absorbing impurities, such as dust, have a tendency to stick at the snowpack surface during spring melt (e.g. Clarke and Noone, 1985; Conway et al., 1996; Doherty et al., 2010, 2013; Sterle et al., 2013; Svensson et al., 2013). Confined to the top centimeters of the snowpack, the BC concentrations in the snow during the melt have been measured to increase by

a factor of 2–7 (Doherty et al., 2013; Sterle et al., 2013). Doherty et al. (2013) found an even higher amplification factor of ∼ 10–15, when melting snow BC concentrations were compared to the concentrations from earlier in the year at a site near Dye-2, on the Greenland ice sheet.

Due to the chosen set-ups for our experiments, where higher amounts of soot were deposited on the snow surface, it was not expected that the EC concentrations would increase during melt. However, 9 days after deposition, 36 and 43 % (at two different experimental spots) of the initial soot particles were observed at the snow surface. It is also worth noting that in one of the spots (spot N) there was a substantial increase in EC concentration between the 9th and the 16th day, with the EC concentration increasing from 529 to 859 ppb, while the other spot had a marginal increase from 730 to 756 ppb during that time. The reason for this increase is unknown. Conway et al. (1996) reported that the soot concentration (for both the hydrophobic and hydrophilic soot) in the surface snow layer decreased by 2 orders of magnitude over the course of 10 days. Noteworthy though, is that Conway et al. (1996) used amounts of soot that were much higher compared to our EC concentrations.

3.2 Albedo

In SoS2011, the broadband albedos of the contaminated and the reference snow, following the initial soot deposition, were 0.52 and 0.83, respectively. In Fig. 3a, the temporal evolution of the albedo from the contaminated and clean snow is presented as daily averages at solar noon ± one hour. As expected with natural snow aging, the reference site's albedo decreased overall from 0.83 to 0.65 over the first month of observations. During this period, there were a few snow fall events, leading to the fluctuations in the albedo. Following this period, the albedo decreased rapidly until the snowpack had completely melted on 12 April. The fluctuations in the soot-contaminated snow albedo were larger than those for the reference site, with the snow fall events increasing the albedo to similar values as the reference site. Following the snowfalls, the new snow melted faster over the contaminated snow than over the reference snow. After

this melt, the contaminated snow layer would be visible again with its lower albedo. Noteworthy is also a large snowfall event on 20 March that covered the albedo measurement devices. The snow accumulated onto the upward-looking sensor hindering the instrument from proper collection of photons, resulting in irradiance values close to zero, and consequently albedo values exceeding the unity.

For SoS2013, the trend in the albedo was similar to that shown in Fig. 3 for SoS2011. Following soot deposition, the albedo was lowest at the spots with the highest amount of soot and vice versa, the albedo was highest at the spots with the lowest amount of soot (see Table 1).

The albedo time series in Fig. 3b show a sharp increase of 0.23 in albedo of the most contaminated spot during the first two measurements days. This increase could be explained by the fact that after deposition the soot particles sunk into the snow surface, within minutes of deposition, as visually observed. The soot particles sunk during the day at elevated solar radiation, and thereafter stopped sinking during the nights when the temperature was well below zero (indicated by the temperature minimum in Fig. 3b). The soot particles probably became stagnant after this initial sinking, and with the snow surface melting, but particles not being washed down with the meltwater, they became closer to the surface, affecting the albedo again. The albedo started to decrease again on the third day of measurements. On 14 April, a snow shower put few centimeters of fresh snow on the snowpack. A distinct increase in albedo was observed between 14 and 15 April. This increase was not as pronounced for the other spots. Similar to the snowfall events in SoS2011, the melting of the fresh snow and decrease in albedo occurred fastest on the spot where the soot concentration was highest. Another event with an increase in the albedo, visible in all spots, occurred on 18 and 19 April. At this time, the precipitation was in the form of rain. The increase in albedo can possibly be due to rain lowering the density of the BC-containing snowpack (Meinander et al., 2014), meaning lower water content in the sooted snow and resulting in optically smaller snow grains with higher albedo, and/or possibly that some soot particles were lost from the surface at this time. Both of these cases would lead to an

enhanced albedo of the snowpack. On 22 April, the albedo began to decrease rapidly starting with the spot with the highest BC concentration changing its albedo from 0.55 to 0.15 during 72 h. The spots with lower BC concentrations followed this rapid decrease in albedo a few days later. The temporal variation of the albedo at Spot S9 (second highest EC concentration) and the contaminated reference spot (S9B) were nearly identical during this fast albedo reduction. The albedo decreased earlier at the spot with the lowest EC concentration (S10) than at the spot with the second lowest EC concentration (S8). However, since snow samples were not collected for determination of the EC concentrations for these spots at this time, their concentrations are unknown. Further, it is questionable how much of an impact the BC has on the snowmelt (especially with lower EC concentrations) during this time when the snowpack height was lower than ~ 30 cm as one would expect the albedo of the underlying ground to have the strongest effect on snow melt.

3.3 Physical snow characteristics

During SoS2011, the melting rates of the snow at the reference site and at the soot contaminated spot were 3 and 7 cm day^{-1}, respectively. From the snow pits dug and studied one month after soot deposition in SoS2011, it was evident that the snow containing the soot had experienced further changes than the reference snow (Fig. 2a–d). The soot doped snow had transformed to a more homogenous snowpack containing rounded polycrystal snow grains, whereas the grain shapes of the reference snow were more heterogeneous. Similarly, the hardness test revealed a more uniform pattern in the sooted snow, while the reference site was more diverse. The snow depth for the dirty snowpack was at that time 35 cm, while the clean snow had a depth of 50 cm. Both of the pits had a layer of freshly fallen snow (4 cm deep at the reference site, and 2 cm deep at the sooted snow), containing 0.5 mm snow grains. The remaining snow had a snow grain size of 2 mm, except for the bottom 5 cm at the reference site, where the snow grain size was 1 mm. The snow density was practically the same for the two snow pits. The density varied between 340–400 kg m^{-3} in the top part of snowpack

and was about 460 kg m^{-3}. Since the snowpack had brittle layers and also some very loose layers, it was difficult to conduct the density measurements. Therefore density data were obtained from only a few measurements.

At the time of the soot deposition during SoS2013, the surface layer of the clean reference snow had a depth of 1 cm containing irregular precipitation particles with thereunder several layers with rounded and faceted crystals produced by snow metamorphism (Fig. 2e–g). The average visual grain size varied between 0.5 mm at the surface, while the bottom contained 2.8 mm grain sizes (this was a depth hoar). Four days later, the snow pit work in two of the sooted spots (Spot 5 and Spot 7) revealed that a hard melt-freeze layer had developed near the snow surface, followed by a layer of faceted snow crystals and another melt-freeze layer (Fig. 2f and g). The average surface grain sizes at these spots were estimated to be 0.5 and 1 mm, respectively. In addition, larger aggregates produced by snow grains melting and refreezing together were observed near the surface. However, snow pit work done two days earlier in the nearby mire and forested areas, revealed the same kind of snow stratification indicating that the melt-freeze layers were not only produced by the presence of light absorbing impurities but were caused by the changes in the weather conditions as well. It is, however, hypothesized that the impurities may enhance the development of surface crusts by enhancing the snow melt during the sunny hours, while the air temperature still drops below zero at night time. Eleven days after the first measurements, the snow characteristics of these two sooted spots plus a clean reference snow were measured again. At that time, the snow melt had already started as the temperature of the whole snowpack was 0 °C, and snow grain types of rounded melt forms were recorded. The average surface grain size in all three spots was estimated to be 1 mm.

During SoS2013, we observed that the soot containing snow lowered the density of melting snow (Meinander et al., 2014). We also observed that light-absorbing impurities deposited on snow enhance the immediate metamorphosis under strong sunlight (Peltoniemi et al., 2015). After soot deposition, the contaminated snow surface is darker

than the pure snow in all viewing directions, but as stated above, we observed the soot particles sinking into the snow, thus increasing its surface roughness.

3.4 SNICAR modelling and comparison to SoS data

The SoS experimental data points are compared to SNICAR model simulations of the effect of BC concentrations on the snow albedo as shown in Fig. 4. In addition, the SoS experimental data was fitted with two different logarithmic fits, one for EC concentrations lower than 1 ppm and one for all of the EC concentrations used in the SoS campaigns. For EC concentrations below 1 ppm, the relation could be described as:

$$\text{albedo} = -0.046 \ln(\text{EC}) + 0.71, \quad (2)$$

whereas for the whole EC range used in SoS could be described as:

$$\text{albedo} = -0.087 \ln(\text{EC}) + 0.66. \quad (3)$$

This parameterization describes the reduction of the broadband snow albedo in response to increased EC loading, immediately following soot deposition. After 72 h of soot deposition, with no precipitation meanwhile, the parameterization changed only marginally, when applying either EC concentrations below 1 ppm or the entire EC range. The coefficient (and intercept) values were −0.045 (0.71) and −0.073 (0.67), respectively. Thus, without precipitation our parameterization was still valid after 72 h.

The comparison between the SNICAR model results and the SoS data shows that the results agree best when an effective snow grain radius of 270 µm is used in the model. With an effective radius of 750 µm, SNICAR overestimates the albedo reduction (with the exception of the most contaminated spot from SoS2013). Similarly, when the BC-coated option is chosen, the SNICAR model overestimates the albedo reduction.

During SoS2011 the albedo at the reference site (0.83) could not be reproduced with the SNICAR model (with SoS2011 data as input parameters). The SNICAR-simulated albedo varies from 0.78 (MAC-factor 0.3 and grain effective radius 270 µm) to 0.71

(MAC-factor 1 and grain effective radius 750 µm). However, tuning the grain effective radius to 100 µm and a MAC-factor of 0.3 produces an albedo of 0.83. Since accurate snow grain measurements were not conducted in SoS2011, as well as an accurate soot characterization, this is a realistic possibility. Thus, accurate knowledge of the snow grain size is crucial to properly model the snow albedo. Similarly, also in SoS2012, the measured albedo (0.92) could not be reproduced with SNICAR with our input parameters. The reason for this discrepancy is unknown.

The reductions of modelled albedo with the SNICAR model reflect the conditions that exist right after soot deposition in these experiments. The temporal variation, and the associated snow processes affected by the presence of BC in the snow are not supported by these simulations. Here the focus was on dry deposition of impurities on cold snow surfaces.

4 Summary, conclusions, and future recommendations

A series of experiments was conducted to study the effect of BC on snow properties. Combustion generated soot was deposited onto a natural snowpack, followed by monitoring the albedo and snow physical characteristics throughout spring melt. A clear effect on the albedo and snow melt was visible when soot concentrations of 1000 ppb were used, whereas it was more difficult to attribute the soot's effect when lower concentrations of 100 ppb were used (or difficult to attribute with our rough measurement methods). The effect of 100 ppb should not be, however, overlooked as their 1–2 % change in albedo can have detrimental effects on the overall climate (for example in the Arctic). Our experimental data generally agreed with the SNICAR model when tuned to a specific effective snow grain size radius. However, the SNICAR model failed or had difficulties to simulate the high albedo in the undisturbed reference site in SoS2011 and SoS2012. For the experimental data there was an agreement between the SoS2011 and SoS2013 data points. This is despite the fact that these experiments were conducted at two different years and in two different geographical areas with different snow

conditions, as well as different origins of soot and different methods used to deposit the soot onto the snow surface.

We observed an increase in melting rates for the soot-contaminated snowpack as compared to the reference site (reflected by the fact that the soot containing spot melted one week earlier than the reference snow). It is noted that this observation refers to a situation during SoS2011 when the concentration of soot was very high. Also, during SoS2011 the composition of the snow grains was observed to change to a more homogenous pattern drastically in the contaminated site compared to the reference site one month after the initial soot deposition. We also observed a decrease of the density of melting snow in the presence of soot in SoS2013 (Meinander et al., 2014). It was confirmed that a large fraction of soot particles remained at the snow surface (5 cm top layer), with about 40 % of the soot particles remaining in the surface layer at 9 and 16 days after the initial soot deposition. In both experiments, we observed the albedo of the (most) contaminated snow to return to a value lower than that of the reference snow shortly after any snowfall events.

The experience gained during the three SoS experiments leads to the following recommendations for future studies:

1. Focus on lower BC concentrations (< 500 ppb), to add more data for situations where ambient BC in snow concentrations typically are observed and compare these with the SNICAR model.
2. Produce experimental spots on a location where the underlying surface albedo is similar and preferably high, to avoid surface effects on the melting rate.
3. It is difficult to deposit soot onto the snow in a controlled way with the two methods used here. A development of different blowing system should be considered.
4. Experiments should be made over a longer time period. In SoS2013 intense melting began basically as soon as the soot has been deposited onto the snow. It would be of interest to deposit the soot onto the snow surface earlier in the winter season and before snow melt is expected to start to observe BC's interaction with the snowpack also before the onset of intense melting.
5. More detailed and regular measurements to follow the changes in the various parameters for the experiment, rather than infrequent follow-up. Parameters especially interesting to follow would be the melt-rate for snow with different BC concentrations; the change in BC aerosol diameter after deposition to the snow and its evolution with melting.
6. Additional studies with depositing other light-absorbing impurities, such as dust, onto the snow to compared their differences with BC's and the effect they have on the snowpack.
7. Lastly, we recommend having additional (clean) reference sites, doubled down welling radiation measurements, and even more detailed snow property measurements for the top most mms, in order to better attribute BC's effect on snow properties.

Acknowledgements. We would like to thank Antti Aarva for helping us with numerous issues throughout these experiments. The work of the technical staff at FMI, Sodankylä, during SoS2013 is very much appreciated. The Chimney sweeping company (Consti Talotekniikka Oy) is acknowledged for supplying us with the soot. This work has been supported by the Academy of Finland through the projects: Arctic Absorbing Aerosols and Albedo of Snow (project no. 3162), and the Electromagnetic Wave Scattering in a Complex Random Medium (project no. 260027). This work has also been supported by the EU LIFE+ project MACEB (project no. LIFE09 ENV/FI/000572the European Commission ERC Advanced Grant No. 320773 (SAEMPL); the Maj and Tor Nessling Foundation (projects 2012456 and 2013093); the KONE foundation; and the Nordic research and innovation initiative Cryosphere–Atmosphere Interactions in a Changing Arctic Climate (CRAICC).

References

Birch, M. E. and Cary, R. A.: Elemental carbon-based method for monitoring occupational exposures, to particulate diesel exhaust, Aerosol Sci. Tech., 25, 221–241, 1996.

Bond, T. C. and Bergstrom, R. W.: Light absorption by carbonaceous particles: an investigative review, Aerosol Sci. Tech., 39, 1–41, doi:10.1080/02786820500421521, 2005.

Bond, T. C., Doherty, S. J., Fahey, D. W., Forster, P. M., Berntsen, T., DeAngelo, B. J., Flanner, M. G., Ghan, S., Kärcher, B., Koch, D., Kinne, S., Kondo, Y., Quinn, P. K., Sarofim, M. F., Schultz, M. G., Schulz, M., Venkataraman, C., Zhang, H., Zhang, S., Bellouin, N., Guttikunda, S. K., Hopke, P. K., Jacobson, M. Z., Kaiser, J. W., Klimont, Z., Lohmann, U., Schwarz, J. P., Shindell, D., Storelvmo, T., Warren, S. G., and Zender, C. S.: Bounding the role of black carbon in the climate system: a scientific assessment, J. Geophys. Res., 188, 5380–5552, doi:10.1002/jgrd.50171, 2013.

Brandt, R. E., Warren, S. G., and Clarke, A. D.: A controlled snowmaking experiment testing the relation between black-carbon content and reduction of snow albedo, J. Geophys. Res., 116, D08109, doi:10.1029/2010JD015330, 2011.

Cavalli, F., Viana, M., Yttri, K. E., Genberg, J., and Putaud, J.-P.: Toward a standardised thermal-optical protocol for measuring atmospheric organic and elemental carbon: the EUSAAR protocol, Atmos. Meas. Tech., 3, 79–89, doi:10.5194/amt-3-79-2010, 2010.

Clarke, A. D. and Noone, K. J.: Soot in the Arctic snowpack: a cause for perturbations in radiative transfer, Atmos. Environ., 19, 2045–2053, 1985.

Conway, H., Gades, A., and Raymond, C. F.: Albedo of dirty snow during conditions of melt, Water Resour. Res., 32, 1713–1718, 1996.

Dagsson-Waldhauserova, P., Arnalds, O., and Olafsson, H.: Long-term variability of dust events in Iceland (1949–2011), Atmos. Chem. Phys., 14, 13411–13422, doi:10.5194/acp-14-13411-2014, 2014.

Dagsson-Waldhauserova, P., Arnalds, O., Olafsson, H., Hladil, J., Skala, R., Navratil, T., Chadimova, L., and Meinander, O.: Snow–dust storm: unique case study from Iceland, March 6–7, 2013, Aeolian Res., 16, 69–74, doi:10.1016/j.aeolia.2014.11.001, 2015.

Dahlkötter, F., Gysel, M., Sauer, D., Minikin, A., Baumann, R., Seifert, P., Ansmann, A., Fromm, M., Voigt, C., and Weinzierl, B.: The Pagami Creek smoke plume after long-range transport to the upper troposphere over Europe – aerosol properties and black carbon mixing state, Atmos. Chem. Phys., 14, 6111–6137, doi:10.5194/acp-14-6111-2014, 2014.

Doherty, S. J., Warren, S. G., Grenfell, T. C., Clarke, A. D., and Brandt, R. E.: Light-absorbing impurities in Arctic snow, Atmos. Chem. Phys., 10, 11647–11680, doi:10.5194/acp-10-11647-2010, 2010.

Doherty, S. J., Grenfell, T. C., Forsström, S., Hegg, D. L., Brandt, R. E., and Warren, S. G.: Observed vertical redistribution of black carbon and other insoluble light-absorbing particles in melting snow, J. Geophys. Res., 118, 1–17, doi:10.1002/jgrd.50235, 2013.

Domine, F., Salvatori, R., Legagneux, L., Salzano, R., Fily, M., and Casacchia, R.: Correlation between the specific surface area and the short wave infrared: SWIR reflectance of snow, Cold Reg. Sci. Technol., 46, 60–68, 2006.

Fierz, C., Armstrong, R. L., Durand, Y., Etchevers, P., Greene, E., McClung, D. M., Nishimura, K., Satyawali, P. K., and Sokratov, S. A.: The International Classification for Seasonal Snow on the Ground, IHP-VII Technical Documents in Hydrology No. 83, IACS Contribution No. 1, UNESCO-IHP, Paris, 2009.

Flanner, M. G., Zender, C. S., Randerson, J. T., and Rasch, P. J.: Present-day climate forcing and response from black carbon in snow, J. Geophys. Res., 112, D11202, doi:10.1029/2006JD008003, 2007.

Forsström, S., Ström, J., Pedersen, C. A., Isaksson, E., and Gerland, S.: Elemental carbon distribution in Svalbard snow, J. Geophys. Res., 114, D19112, doi:10.1029/2008JD011480, 2009.

Forsström, S., Isaksson, E., Skeie, R. B., Ström, J., Pedersen, C. A., Hudson, S. R., Berntsen, T. K., Lihavainen, H., Godtliebsen, F., and Gerland, S.: Elemental carbon measurements in European Arctic snow packs, J. Geophys. Res., 118, 13614–13627, doi:10.1002/2013JD019886, 2013.

Gallet, J.-C., Domine, F., Zender, C. S., and Picard, G.: Measurement of the specific surface area of snow using infrared reflectance in an integrating sphere at 1310 and 1550 nm, The Cryosphere, 3, 167–182, doi:10.5194/tc-3-167-2009, 2009.

Gao, R. S., Schwarz, J. P., Kelly, K. K., Fahey, D. W., Watts, L. A., Thompson, T. L., Spackman, J. R., Slowik, J. G., Cross, E. S., Han, J.-H., Davidovits, P., Onasch, T. B., and Worsnop, D. R.: A novel method for estimating light-scattering properties of soot aerosols using a modified single-particle soot photometer, Aerosol Sci. Tech., 41, 125–135, 2007.

Gardner, A. S. and Sharp, M. J.: A review of snow and ice albedo and the development of a new physically based broadband albedo parameterization, J. Geophys. Res., 115, F01009, doi:10.1029/2009JF001444, 2010.

Grenfell, T. C. and Warren, S. G.: Representation of a nonspherical ice particle by a collection of independent spheres for scattering and absorption of radiation, J. Geophys. Res., 104, 31697–31709, 1999.

Grenfell, T. C., Neshyba, S. P., and Warren, S. G.: Representation of a nonspherical ice particle by a collection of independent spheres for scattering and absorption of radiation: 3. Hollow columns and plates, J. Geophys. Res., 110, D17203, doi:10.1029/2005JD005811, 2005.

Hadley, O. L. and Kirchstetter, T. W.: Black-carbon reduction of snow albedo, Nat. Clim. Change, 2, 437–440, doi:10.1038/nclimate1433, 2012.

Hansen, J. and Nazarenko, L.: Soot climate forcing via snow and ice albedos, P. Natl. Acad. Sci. USA, 101, 423–428, doi:10.1073/pnas.2237157100, 2004.

Heintzenberg, J.: Size-segregated measurements of particulate elemental carbon and aerosol light absorption at remote Arctic locations, Atmos. Environ., 16, 2461–2469, doi:10.1016/0004-6981(82)90136-6, 1982.

ISO 9060:1990: Solar energy – Specification and classification of instruments for measuring hemispherical solar and direct solar radiation, International Organization for Standardization, Geneva, 1990.

Kaspari, S. D., Schwikowski, M., Gysel, M., Flanner, M. G., Kang, S., Hou, S., and Mayewski, P. A.: Recent increase in black carbon concentrations from a Mt. Everest ice core spanning 1860–2000 AD, Geophys. Res. Lett., 38, L04703, doi:10.1029/2010GL046096, 2011.

Kokhanovsky, A. A. and Zege, E. P.: Scattering optics of snow, Appl. Optics, 43, 1589–1602, 2004.

Lavanchy, V. M. H., Gäggler, H. W., Schotterer, U., Schwikowski, M., and Baltensperger, U.: Historical record of carbonaceous particle concentrations from a European high-alpine glacier (Colle Gnifetti, Switzerland), J. Geophys. Res., 104, 21227–21236, 1999.

Legagneux, L., Cabanes, A., and Dominé, F.: Measurement of the specific surface area of 176 snow samples using methane adsorption at 77 K, J. Geophys. Res., 107, 4335, doi:10.1029/2001JD001016, 2002.

Lim, S., Faïn, X., Zanatta, M., Cozic, J., Jaffrezo, J.-L., Ginot, P., and Laj, P.: Refractory black carbon mass concentrations in snow and ice: method evaluation and inter-comparison with elemental carbon measurement, Atmos. Meas. Tech., 7, 3307–3324, doi:10.5194/amt-7-3307-2014, 2014.

McConnell, J. R., Edwards, R., Kok, G. L., Flanner, M. G., Zender, C. S., Salzman, E. S., Banta, J. R., Pasteris, D. R., Carter, M. M., and Kahl, J. D. W.: 20th century industrial black carbon emissions altered arctic climate forcing, Science, 317, 1381–1384, 2007.

Meinander, O., Kazadzis, S., Arola, A., Riihelä, A., Räisänen, P., Kivi, R., Kontu, A., Kouznetsov, R., Sofiev, M., Svensson, J., Suokanerva, H., Aaltonen, V., Manninen, T., Roujean, J.-L., and Hautecoeur, O.: Spectral albedo of seasonal snow during intensive melt period at Sodankylä, beyond the Arctic Circle, Atmos. Chem. Phys., 13, 3793–3810, doi:10.5194/acp-13-3793-2013, 2013.

Meinander, O., Kontu, A., Virkkula, A., Arola, A., Backman, L., Dagsson-Waldhauserová, P., Järvinen, O., Manninen, T., Svensson, J., de Leeuw, G., and Leppäranta, M.: Brief communication: Light-absorbing impurities can reduce the density of melting snow, The Cryosphere, 8, 991–995, doi:10.5194/tc-8-991-2014, 2014.

Ming, J., Cachier, H., Xiao, C., Qin, D., Kang, S., Hou, S., and Xu, J.: Black carbon record based on a shallow Himalayan ice core and its climatic implications, Atmos. Chem. Phys., 8, 1343–1352, doi:10.5194/acp-8-1343-2008, 2008.

Neshyba, S. P., Grenfell, T. C., and Warren, S. G.: Representation of a nonspherical ice particle by a collection of independent spheres for scattering and absorption of radiation: 2. Hexagonal columns and plates, J. Geophys. Res., 108, D17203, doi:10.1029/2002JD003302, 2003.

Ogren, J. A., Charlson, R. J., and Groblckl, P. J.: Determination of elemental carbon in rainwater, Anal. Chem., 55, 1569–1572, 1983.

Peltoniemi, J. I., Manninen, T., Suomalainen, J., Hakala, T., Puttonen, E., and Riihelä, A.: Land surface albedos computed from 650 BRF measurements with a study of conversion formulae, Remote Sensing, 2, 1918–1940, doi:10.3390/rs2081918, 2010a.

Peltoniemi, J. I., Suomalainen, J., Hakala, T., Puttonen, E., Näränen, J., Kaasalainen, S., Torppa, J., and Hirschmugl, M.: Reflectance of various snow types: measurements, modelling and potential for snow melt monitoring, in: Light Scattering Reviews 5: Single Light Scattering and Radiative Transfer, edited by: Kokhanovsky, A. A., Springer Praxis Books, 393–450, doi:10.1007/978-3-642-10336-0, 2010b.

Peltoniemi, J. I., Hakala, T., Suomalainen, J., Honkavaara, E., Markelin, L., Gritsevich, M., Eskelinen, J., Jaanson, P., and Ikonen, E.: Technical notes: a detailed study for the provision of measurement uncertainty and traceability for goniospectrometers, J. Quant. Spectrosc. Ra., 146, 376–390, doi:10.1016/j.jqsrt.2014.04.011, 2014.

Peltoniemi, J. I., Gritsevich, M., and Puttonen, E.: Reflectance and polarization characteristics of various vegetation types, in: Light Scattering Reviews 9: Light Scattering and Radiative Transfer, edited by: Kokhanovsky, A. A., Springer Praxis Books, 257–294, doi:10.1007/978-3-642-37985-7_7, 2015.

Petzold, A., Ogren, J. A., Fiebig, M., Laj, P., Li, S.-M., Baltensperger, U., Holzer-Popp, T., Kinne, S., Pappalardo, G., Sugimoto, N., Wehrli, C., Wiedensohler, A., and Zhang, X.-Y.: Recommendations for reporting "black carbon" measurements, Atmos. Chem. Phys., 13, 8365–8379, doi:10.5194/acp-13-8365-2013, 2013.

Ruppel, M. M., Isaksson, E., Ström, J., Beaudon, E., Svensson, J., Pedersen, C. A., and Korhola, A.: Increase in elemental carbon values between 1970 and 2004 observed in a 300-year ice core from Holtedahlfonna (Svalbard), Atmos. Chem. Phys., 14, 11447–11460, doi:10.5194/acp-14-11447-2014, 2014.

Schwarz, J. P., Gao, R. S., Fahey, D. W., Thomson, D. S., Watts, L. A., Wilson, J. C., Reeves, J. M., Darbeheshti, M., Baumgardner, D. G., Kok, G. L., Chung, S. H., Schulz, M., Hendricks, J., Lauer, A., Kärcher, B., Slowik, J. G., Rosenlof, K. H., Thompson, T. L., Langford, A. O., Loewenstein, M., and Aikin, K. C.: Single-particle measurements of midlatitude black carbon and light-scattering aerosols from the boundary layer to the lower stratosphere, J. Geophys. Res., 111, D16207, doi:10.1029/2006JD007076, 2006.

Stephens, M., Turner, N., and Sandberg, J.: Particle identification by laser-induced incandescence in a solid-state laser cavity, Appl. Optics, 42, 3726–3736, 2003.

Sterle, K. M., McConnell, J. R., Dozier, J., Edwards, R., and Flanner, M. G.: Retention and radiative forcing of black carbon in eastern Sierra Nevada snow, The Cryosphere, 7, 365–374, doi:10.5194/tc-7-365-2013, 2013.

Suomalainen, J., Hakala, T., Peltoniemi, J., and Puttonen, E.: Polarised multiangular reflectance measurements using Finnish Geodetic Institute Field Goniospectrometer, Sensors, 9, 3891–3907, doi:10.3390/s90503891, 2009.

Svensson, J. Ström, J., Hansson, M., Lihavainen, H., and Kerminen, V.-M.: Observed metre scale horizontal variability of elemental carbon in surface snow, Environ. Res. Lett., 8, 034012, doi:10.1088/1748-9326/8/3/034012, 2013.

Torres, A., Bond, T. C., Lehmann, C. M. B., Subramanian, R., and Hadley, O. L.: Measuring organic carbon and black carbon in rainwater: evaluation of methods, Aerosol Sci. Tech., 48, 239–250, doi:10.1080/02786826.2013.868596, 2014.

Warren, S. G. and Wiscombe, W. J.: A model for the spectral albedo of snow. II: Snow containing atmospheric aerosols, J. Atmos. Sci., 37, 2734–2745, 1980.

Wiscombe, W. J. and Warren, S. G.: A model for the spectral albedo of snow. I: Pure snow, J. Atmos. Sci., 37, 2712–2733, 1980.

World Meteorological Organization: Guide to Meteorological Instruments and Methods of Observation WMO-No. 8, Edition 2008 Updated in 2010, Secretariat of the World Meteorological Organization, Geneva, Switzerland, 2012.

Xu, B., Cao, J., Hansen, J., Yao, T., Joswiak, D. R., Wang, N., Wu, G., Wang, M., Zhao, H., Yang, W., Liu, X., and He, J.: Black soot and the survival of Tibetan glaciers, P. Natl. Acad. Sci. USA, 106, 22114–22118, 2009.

Table 1. Spots made in SoS2013 and the corresponding EC values and variation from the snow samples taken.

Spot nr	Number of samples	Average EC (ppb)	EC variation ±	Albedo immediately following soot deposition
1	3	6417	35 %	0.41
5	4	1689	8 %	–*
7	4	1465	2 %	–*
8	4	489	40 %	0.75
9	4	1026	20 %	0.70
10	4	232	28 %	0.77
9B (reference)	2	554	22 %	0.75

* no albedo measurements conducted for these spots.

Table 2. Temporal evolution of the concentrations of soot particles for two spots in SoS2013.

Sampling date	Sample interval (cm)	Spot 7 EC (ppb)	% of total	Spot 5 EC (ppb)	% of total
8 Apr 2013	0–7	**1465**		**1689**	
17 Apr 2013	0–5	529	71 %	730	69 %
	5–10	7	1 %	118	11 %
	10–15	0	0 %	88.4	8 %
	15–20	74	10 %	64.5	6 %
	20–25	136	18 %	55.9	5 %
	total	**746**		**1057**	
24 Apr 2013	0–5	859	64 %	756	
	5–10	475	36 %	–*	
	total	**1334**		**756**	

* Indicates no EC concentration since the total snow column was 7 cm at that time in that spot.

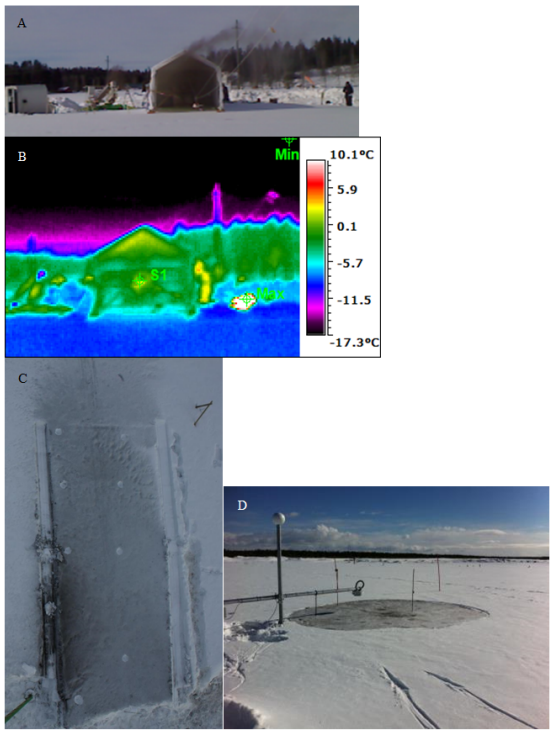

Figure 1. (a) Photograph of soot production and deposition in SoS2011; **(b)** thermo graphic image of the temperature ranges during deposition in SoS2011, showing temperatures below 0 °C inside the chamber; **(c)** rectangular soot spot in SoS2011 photographed from above after removing the chamber; **(d)** monitoring setup of one of the spots after soot deposition in SoS2013.

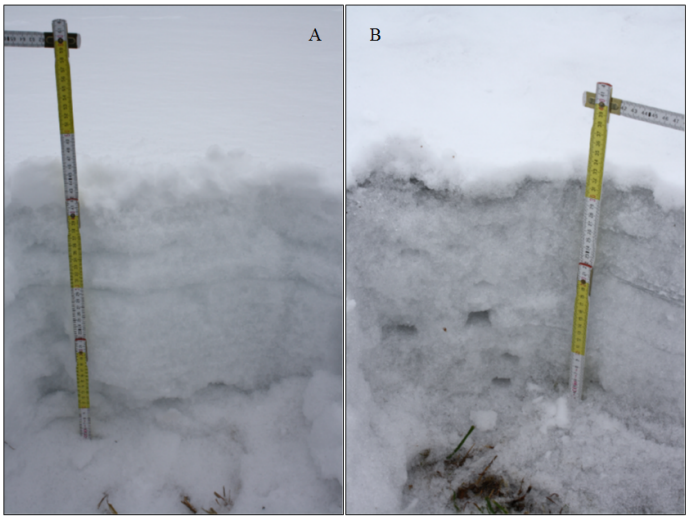

Figure 2.

B

Surface 0 (cm)		Morphological classification subclass shape	Hardness test	Shape code	Size (mm)
Depth	4	rounded	4 fingers	RGlr	0.5-0.7
	9	faceted and some cup shaped	1 finger	FCsf	2
	15	rounded polycrystals	pencil	MFpc	2
	16	refrozen layer, rounded crystals	knife		
	45	rounded by melting some faceted still left	1 finger	FCxr	2
	50	rounded polycrystals	pencil	MFpc	1

Figure 2.

C

Surface 0 (cm)		Morphological classification subclass shape	Hardness test	Shape code	Size (mm)
Depth	2	rounded	4 fingers	RGlr	0.5
	5	rounded polycrystals	1 finger	MFpc	2
	35	rounded polycrystals	pencil	MFpc	2

Figure 2.

E

Surface 0 (cm)		Morphological classification subclass shape	Hardness test	Shape code	Size (ave) (mm)	Size (max) (mm)	Size (min) (mm)	wetness
Depth	1	Irregular crystals	fist	Ppir	0.5	0.8	0.3	dry
	8	Faceted rounded particles	fist	RGxf	1.0	1.5	0.3	dry
	1	Rounding faceted particles	fist	FCxr	1.0	2.5	0.5	dry
	6	Rounding faceted particles	fist	FCxr	1.0	1.8	0.3	dry
	6	Solid faceted particles	4 fingers	FCso	1.5	3.3	0.8	dry
	10	Solid faceted particles	fist	FCso	2.0	3.0	0.8	dry
	8	Solid faceted particles	1 finger	FCso	1.3	2.5	0.5	dry
	13	Hollow cups +Chains of depth hoar	fist	DHcp + DHch	2.5	4.0	1.0	dry
	12	Hollow cups	knife	DHcp	2.8	5.0	1.0	dry

Figure 2.

F

Surface 0 (cm)		Morphological classification subclass shape	Hardness test	Shape code	Size (ave) (mm)	Size (max) (mm)	Size (min) (mm)	wetness
Depth	1	Melt-freeze crust	pencil	MFcr	0.5	1.5	0.3	moist
	2	Near surface faceted particles	fist	FCsf	1.3	2.0	0.8	dry
	10	Rounding faceted particles	fist	FCxr	1.3	2.0	0.8	dry
	3	Melt-freeze crust	1 finger	MFcr	0.8	2.0	0.5	dry
	5	Rounded Grains	1 finger	RG	1.0	1.5	0.8	dry
	7	Faceted Crystals	fist	FC/DH	1.5	3.0	0.8	dry
	2	Rounded Polycrystals/ Melt-freeze crust	pencil	MFpc/MFcr	1.0	3.0	0.8	dry
	6	Large rounded particles	pencil	RGlr	1.0	1.5	0.3	dry
	8	Faceted Crystals/Depth Hoar	fist	FC/DH	1.5	3.5	0.8	dry
	4	Depth Hoar	fist	DH	2.0	4.0	1.0	dry
	4	Depth Hoar/Melt Forms	ice	DH/MF	2.5	3.5	0.8	dry
	4	Depth Hoar	fist	DH	3.0	4.0	0.5	dry

Figure 2.

G

Surface 0 (cm)		Morphological classification subclass shape	Hardness test	Shape code	Size (ave) (mm)	Size (max) (mm)	Size (min) (mm)	wetness
	0.5	Melt-freeze crust	knife	MFcr	1.0	1.5	0.8	dry
	2.0	Rounding faceted particles	fist	FCxr	1.3	1.8	0.5	dry
	0.5	Melt-freeze crust	1 finger	MFcr	1.3	1.5	1.0	dry
	9.5	Rounding faceted particles	fist	FCxr	0.8	1.5	0.5	dry
D	0.5	Melt-freeze crust	knife	MFcr	0.8	1.5	0.3	dry
e	3.5	Rounding faceted particles	fist	FCxr	0.8	1.5	0.5	dry
p	9.0	Rounding depth hoar	fist	DHxr	2.0	3.0	0.8	dry
t	11.0	Melt-freeze crust	1 finger	DHxr	1.3	2.5	0.5	dry
h	10.0	Hollow cups	4 fingers	DHcp	2.0	4.0	1.3	dry

Figure 2. Snow pits from SoS2011 **(a–d)** and SoS2013 **(e–g)**. **(a)** Photograph of the clean reference snow about one month after deposition of the soot to the snow in SoS2011; **(b)** photograph of soot contaminated snow at the same time, **(c)** snow pit report from the reference snow at this time; **(d)** snow pit report from the snow containing the soot. In both of the pictures, a recent snowfall with few centimeters of fresh snow can be seen at the top of the snowpack. **(e)** Snow pit report from the reference snow on 6 April in SoS2013; **(f)** snow pit report from spot S5 on 10 April; **(g)** snow pit report from spot S7 on 10 April.

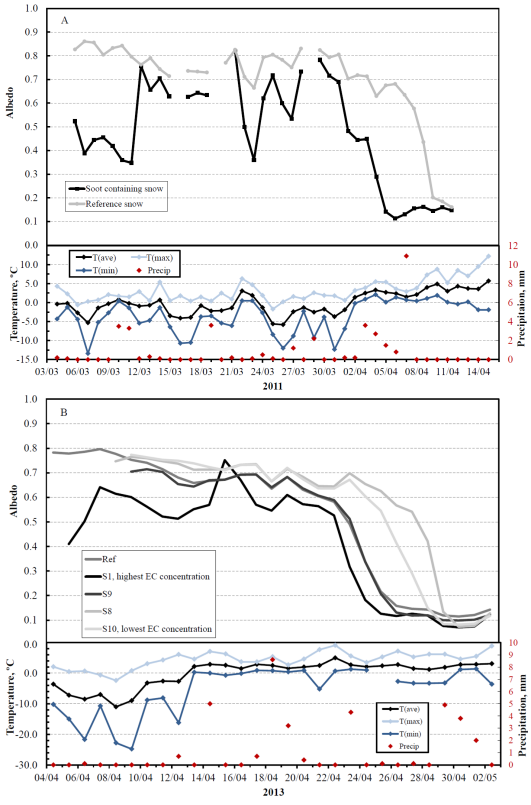

Figure 3. Albedo time series and meteorological conditions during the experiments, **(a)** SoS2011; **(b)** SoS2013.

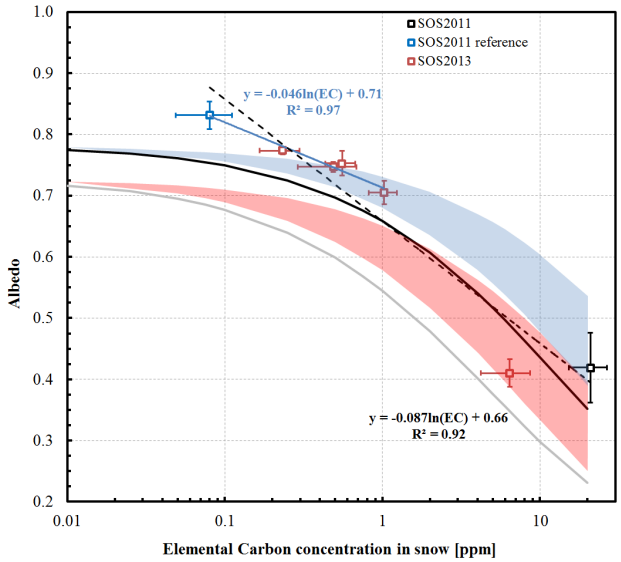

Figure 4. Broadband albedo with corresponding EC concentrations from SoS experiments and the modelled SNICAR albedos. Boxes with the whiskers represent measurements (Black = Nurmijärvi, 2011, Blue = Natural snow, Nurmijärvi, 2011, Red = Sodankylä, 2013). SNICAR model runs are indicated in shaded red and blue bands, with measured SoS2013 data as input parameters. Red shaded band corresponds to a snow grain effective radius of 750 µm, with BC mass absorption cross-section at λ = 550 nm of 7.5 and of 2.25 $m^2 g^{-1}$, as lower and upper limit, respectively. Blue shaded band corresponds to a snow grain effective radius of 274 µm, with BC mass absorption cross-section at λ = 550 nm of 7.5 and of 2.25 $m^2 g^{-1}$, as lower and upper limit, respectively. Blue line is fitted to EC concentrations below 1 ppm, while black dashed line includes all data points. Black solid line refer to 270 µm grain radius and the BC-coated option; while grey solid line refer to 750 µm grain radius and the BC-coated option.